


Article

The Effect of Hydrogen on Pore Formation in Aluminum Alloy Castings: Myth Versus Reality

Murat Tiryakioğlu 

Jacksonville University; Jacksonville, FL 32211, USA; mtiryak@ju.edu; Tel.: +1-904-256-7640

Received: 17 February 2020; Accepted: 9 March 2020; Published: 12 March 2020



Abstract: The solubility of hydrogen in liquid and solid aluminum is reviewed. Based on classical nucleation theory, it is shown that pores cannot nucleate either homogeneously or heterogeneously in liquid aluminum. Results of in situ studies on pore formation show that pores appear at low hydrogen supersaturation levels, bypassing nucleation completely. The results are explained based on the bifilm theory introduced by Prof. John Campbell, as this theory is currently the most appropriate, and most likely, the only mechanism for pores to form. Examples for the effect of hydrogen on pore formation are given by using extreme data from the literature. It is concluded that a fundamental change in how hydrogen is viewed is needed in aluminum casting industry.

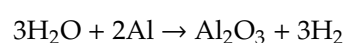
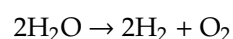
Keywords: supersaturation; fracture pressure; nucleation; bifilm theory; John Campbell

1. Introduction

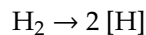
There are many studies in the literature in which pores have been shown to degrade mechanical properties, such as tensile strength [1–13], elongation [6–8,11,14–16], and fatigue life [17–24] of aluminum alloy castings. Moreover, pores have been observed [25] in situ to initiate hot tears, which are common in high strength cast aluminum alloys, such as the Al-Cu system. Additionally, pores can lead to rejection of the aluminum castings during final nondestructive inspection, such as x-ray. Therefore, understanding pore formation is paramount to lowering production costs, increasing their quality and performance, and consequently their wider use. It is understandable why prevention or at least minimization of the number and size of pores has been the main emphasis of foundry engineering research for several decades. Casting processes such as squeeze casting and post-casting processes such as hot isostatic pressing have been used to prevent and heal the pores in castings, respectively. However, these efforts seem to be misguided as they have failed to address the root cause of pores, i.e., inclusions, mainly bifilms. This paper is motivated by this disconnect between the root cause of pores and the steps taken in practice to eliminate them. First, hydrogen solubility in liquid and solid aluminum is discussed. Classical nucleation theory is applied to formation of hydrogen pores in aluminum castings. Finally, hydrogen supersaturation in both liquid and solid aluminum is assessed by using data from the literature, including extreme data for damaged as well as clean melts. A proof-by-contradiction method is used to compare assumptions, observations, and the principles of physics, and to determine the most appropriate mechanism of hydrogen pore formation.

2. Hydrogen in Liquid Aluminum

Hydrogen is the only gas known to be soluble in liquid aluminum. Hydrogen absorption into liquid aluminum is due to the decomposition moisture in air as well as the oxidation of aluminum:



The diatomic hydrogen gets dissolved in aluminum as:



Although hydrogen solubility is much less in aluminum, both in liquid and solid states, than Fe, Cu and Mg [26], hydrogen has been treated as the main culprit for pore formation in aluminum castings because of the significant difference in the solubility of hydrogen in liquid and solid aluminum at its melting temperature. Many researchers and practitioners have hypothesized that the rejection of hydrogen by solidifying aluminum into the mushy zone results in the local hydrogen concentration to exceed the equilibrium concentration, which results in immediate pore formation. We will address the hypothesis of immediate pore formation later. Let us now discuss solubility of hydrogen in aluminum.

The equilibrium concentration, i.e., solubility of hydrogen, $S_{\text{eq}[\text{H}]}$, in aluminum is expressed in the Arrhenius form as:

$$S_{\text{eq}[\text{H}]} = S_{\text{o}[\text{H}]} \cdot \sqrt{P_{\text{H}}} \cdot e^{\frac{-\Delta H}{RT}} \quad (1)$$

where $S_{\text{o}[\text{H}]}$ is solubility coefficient, P_{H} is the partial pressure of hydrogen, ΔH is the enthalpy of solution, R is the gas constant and T is absolute temperature. The dependence of solubility of a diatomic gas in a liquid or solid solvent on the square root of its partial pressure is known as Sievert's law [27]. The linear increase in solubility with the square root of P_{H} has been shown to be valid in liquid [28,29] as well as solid [30] aluminum.

In most of the literature, solubility of hydrogen in liquid aluminum has been expressed in milliliters (or cubic centimeters) of diatomic hydrogen dissolved in 100 g of aluminum, at a pressure of 1 atmosphere (101,325 Pa) and a temperature of 0 °C. This unit can be converted to atomic parts per million (appm) for hydrogen as:

$$1 \text{ mL}/100 \text{ g.Al} = 24.08 \text{ appm}$$

Taking the logarithm of Equation (1), and rearranging, the change in solubility of hydrogen with temperature and pressure in liquid pure aluminum is given by;

$$\log\left(\frac{S_{\text{eq}[\text{H}]}}{\sqrt{P}}\right) = \beta_0 - \frac{\beta_1}{T} \quad (2)$$

where $S_{\text{eq}[\text{H}]}$ is given in mL/100 g.Al and P_{H} in atmosphere. For liquid aluminum, the values of β_0 and β_1 are 2.830 and 2675 (K), respectively [31]. For solid aluminum, $\beta_0 = 1.674$ and $\beta_1 = 2849$ (K) [32]. The change in $S_{\text{eq}[\text{H}]}$ with temperature in liquid and solid aluminum at $P = 1$ atm is presented in Figure 1. Note that the equilibrium hydrogen content in liquid aluminum is approximately twenty-two times that in solid aluminum at its melting temperature. This difference has led to speculation among researchers and foundrymen alike that hydrogen is the main enemy of aluminum casting quality. The belief that degassing will solve the main problem in aluminum castings, pores, has however left the foundry industry still struggling with casting quality issues, despite significant investment in and heavy use of degassing units.

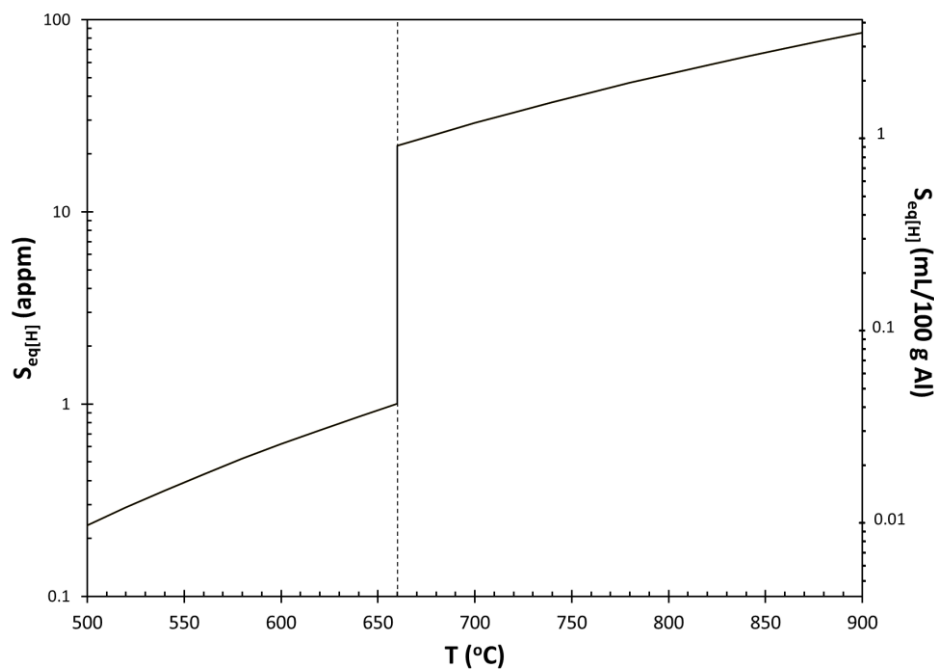


Figure 1. The equilibrium solubility of hydrogen in liquid and solid aluminum as a function of temperature.

3. Hydrogen Pore Formation

3.1. Nucleation

It has been recognized that hydrogen pores cannot nucleate homogeneously [33,34] and therefore, it has been assumed that hydrogen nucleates heterogeneously, mostly on the liquid/solid (L/S) interface [35]. It has been assumed that pores form upon either (i) minimum saturation [36–39], or (ii) a threshold value (e.g., 0.1 mL/100 g Al [40]) has been exceeded. In all cases, usually, a pressure of 1 atmosphere is assumed for ΔP^* . In several studies [36,37,41–44], r^* was assumed to be half of secondary dendrite arm spacing, λ_2 . We will address supersaturation assumption and the threshold hydrogen value later. First, let us review the pressure and critical radius assumptions.

It has been well established, based on classical nucleation theory, that the critical radius above which a pore is stable, r^* is found by:

$$r^* = \frac{-2\sigma}{\Delta P^*} \quad (3)$$

where σ is the surface tension of the liquid (N/m) and ΔP^* is the pressure differential (Pa) and is a negative number. Recently, it has been shown [45,46] by using a combination experimental and molecular dynamics data that the intrinsic fracture pressure of aluminum, $P_{f(\text{int})}$, at the melting temperature is approximately -4 GPa. Hence, by inserting $\Delta P^* = -4$ GPa and $\sigma = 1.03$ N.m [47] in Equation (3), r^* is calculated as 0.515 nm. It should be noted that the critical radius has the same size in both homogeneous and heterogeneous nucleation [48]. Hence, taking half of dendrite arm spacing as r^* is not consistent with the classical nucleation theory.

To attain the pressure necessary for nucleation, the number of hydrogen atoms needed in the embryonic pore, n_{H}^* , is calculated as [49];

$$n_{\text{H}}^* = \frac{-4\pi r^{*3} N_A \Delta P_{\text{het}}^*}{3RT_m \Delta P_{\text{hom}}^*} \quad (4)$$

where ΔP_{het}^* is the heterogeneous nucleation pressure, and ΔP_{hom}^* is the homogeneous nucleation pressure ($= -4$ GPa for aluminum), N_A is Avogadro's number. The plot of Equation (4) is presented in

Figure 2. Note that, in Figure 2, (i) a total of 178 hydrogen atoms are needed in the embryonic pore in homogeneous nucleation, and (ii) $n_{\text{H}}^* \rightarrow 1$ as ΔP_{het}^* is approximately -1 GPa. Hence, it is impossible to have a heterogeneous nucleation pressure of 1.01×10^5 Pa (1 atm) as the number of hydrogen atoms needed for this pressure would be well below one. Let us now discuss whether nucleation, which requires a pressure build up, P_p , between 1 and 4 GPa in the critical sized nucleus, is possible.

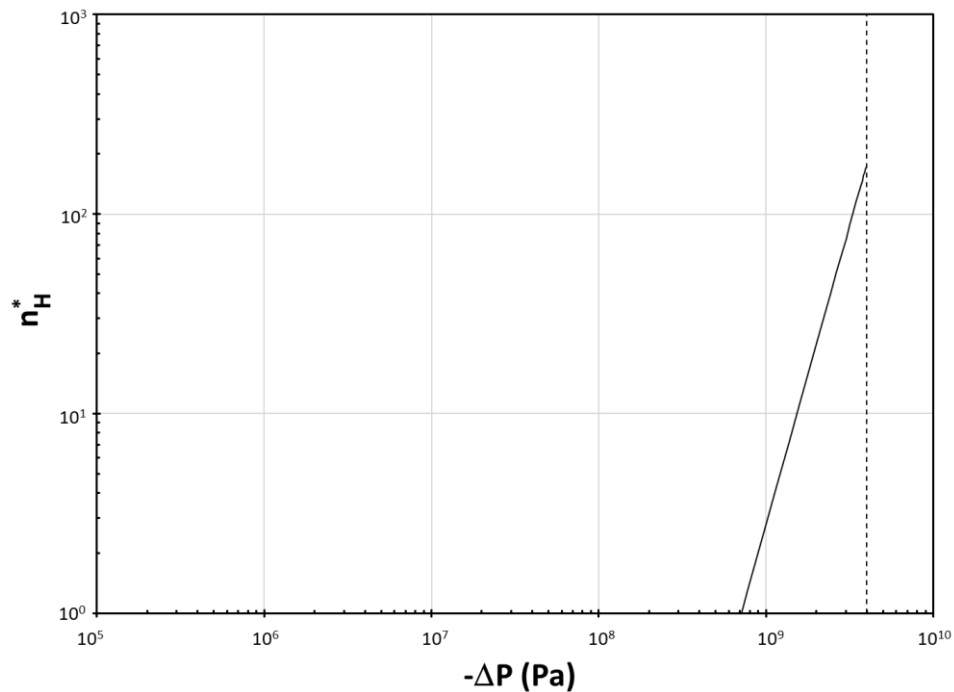


Figure 2. The change in number of hydrogen atoms needed in the critical nucleus with nucleation pressure.

3.2. Stability of Embryonic Pores

When the pressure inside the pore is between 1 to 4 GPa, whether an embryonic pore will be stable can be analyzed in two different ways; (i) by using the Sievert's law, and (ii) by the effect of the pressure on the equilibrium vacancy concentration around the pore.

By using Equation (1), the local equilibrium solubility of hydrogen in aluminum around the pore, $S_{\text{eq}[\text{H}]_{\text{-pore}}}$, can be calculated as;

$$S_{\text{eq}[\text{H}]_{\text{-pore}}} = S_{\text{eq}[\text{H}]} \cdot \sqrt{\frac{P_p}{P_H}} \quad (5)$$

Inserting $P_p = 1$ to 4 GPa and $P_H = 101.3$ kPa in Equation (5), it is found that the solubility of hydrogen is increased by 100 to 200 times locally. Regardless of whether the pore is surrounded by solid or liquid aluminum, the pore would be expected to collapse rather than grow. Therefore, nucleation due to hydrogen supersaturation, either homogeneously or heterogeneously, is again concluded to be impossible, in agreement with the findings of Campbell [50], Shahani, Fredriksson [51], and Yousefian and Tiryakioğlu [52].

Let us still assume that the pressure inside the pore will be equal to or in excess of 1 GPa. This level of pressure will have a profound effect on solid aluminum surrounding the pore. Fukai [53] found that under a pressure of 1–5 GPa and at high temperatures, vacancy concentrations in the order of 10^{-1} can be achieved, as opposed to the equilibrium concentration of 6×10^{-4} in solid aluminum at T_m [54]. Normally, hydrogen atoms are dissolved as interstitials in the aluminum matrix and vacancies in aluminum trap one hydrogen atom [55]. Under pressures that can create superabundant vacancies, however, they can trap up to 10 hydrogen atoms [56]. Therefore, the combination of much higher

concentration of vacancies and the added capacity of each vacancy to trap multiple H atoms will lead to the immediate dissolution of the hydrogen atoms in any embryonic pore. Hydrogen will subsequently remain in solid solution upon solidification, and can even serve to increase strength by pinning down dislocations [57]. Therefore, we again reach the same conclusion that a nucleus of H atoms becomes unstable before it reaches the critical size, resulting in the dissolution of H atoms in aluminum.

4. Hydrogen Supersaturation and Pore Formation Temperature

The temperature of hydrogen pore formation in aluminum and aluminum alloys was investigated in several studies [58–62]. The analysis of these data [63] showed that by the difference between the liquidus and pore formation temperatures, ΔT , followed the lognormal distribution. The density function, f , for this distribution is written as;

$$f(\Delta T) = \frac{1}{\Delta T \cdot \omega_{\Delta T} \cdot \sqrt{2\pi}} \exp\left[-\frac{(\ln(\Delta T) - \theta_{\Delta T})^2}{2\omega_{\Delta T}^2}\right] \quad (6)$$

where $\theta_{\Delta T}$ and $\omega_{\Delta T}$ are the average and standard deviation of the undercooling data after logarithmic transformation, respectively.

Lee and Hunt [64,65] investigated in situ hydrogen pore formation during directional solidification of an Al-10wt.%Cu alloy. They reported that pores could form away from the liquid/solid (L/S) interface, and the temperature at which they appear was not uniform. The histogram of pore formation temperature provided by Lee and Hunt [65] has been reanalyzed. The results have shown that ΔT for hydrogen pore formation follows the lognormal distribution, similar to the results in other studies [58–62]. The distribution, with $\theta_{\Delta T} = 2.10$ and $\omega_{\Delta T} = 0.53$, is presented in Figure 3. Note that a majority of the pores (64.9%) formed within 10 K of the liquidus temperature. It is also significant that x-ray images presented by Lee and Hunt [65] as well as those Liao et al. for an A356 alloy show that pores have formed at temperatures above the liquidus. Hence, hydrogen supersaturation ahead of the advancing solidification front needs to be taken into account, which will be addressed now.

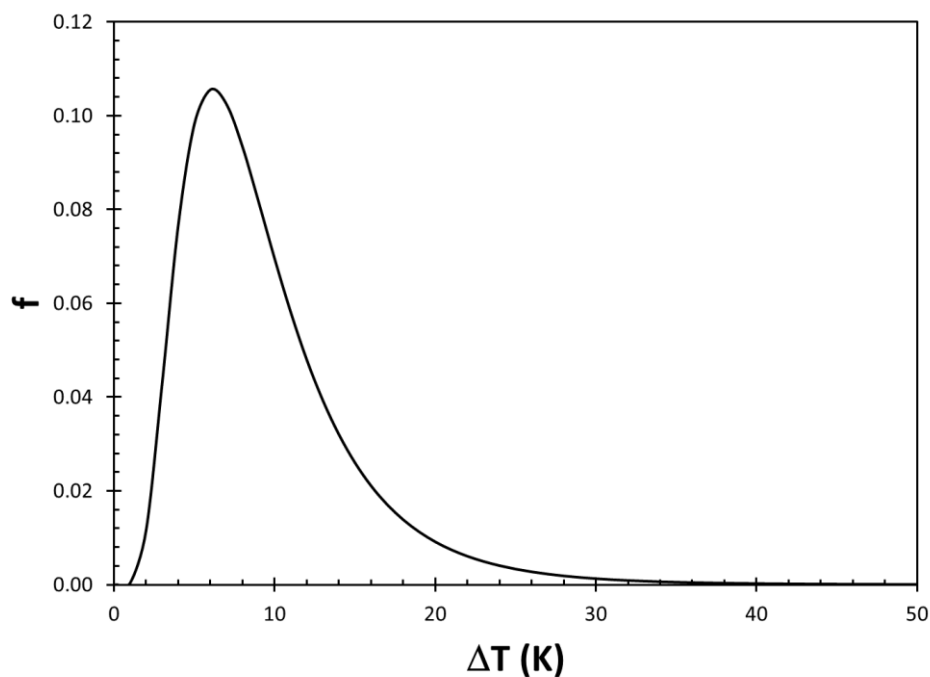


Figure 3. The lognormal distribution for the undercooling below the liquidus temperature for hydrogen pore formation during directional solidification of an Al-10wt.%Cu alloy.

4.1. Hydrogen Supersaturation during Solidification

When the local hydrogen content exceeds the solubility of hydrogen at that temperature, liquid aluminum is in a metastable state. Consequently, there is a driving force to get rid of the excess hydrogen, either by diffusion or pore formation. As discussed above, nucleation of a pore requires that the surface energy barrier be overcome. Hence, the formation of a pore immediately when local hydrogen content exceeds solubility means that there is no surface energy barrier to be overcome, or alternatively, pores only grow, bypassing nucleation.

Hydrogen supersaturation, $S_{s[H]}$, can be quantified by the ratio of the hydrogen content (local or overall) to the hydrogen solubility at the particular temperature. We will first discuss hydrogen supersaturation in liquid aluminum, then shift our attention to supersaturation in solid aluminum.

Lee and Hunt [65] calculated the hydrogen supersaturation in liquid aluminum, $S_{s[H]-liq}$, at the temperature of pore formation as;

$$S_{s[H]-liq} = \frac{1}{1 - (1 - k_H)f_s} \quad (7)$$

where k_H is the partition coefficient for hydrogen and f_s is the solid fraction, calculated from the Scheil–Gulliver nonequilibrium solidification model;

$$f_s = 1 - \left(\frac{T - T_m}{T_{liq} - T_m} \right)^{\frac{1}{k_0 - 1}} \quad (8)$$

where T_m is the melting point of aluminum (933 K), T_{liq} is the liquidus temperature for the alloy chemical composition (K), and k_0 is the partition coefficient for the alloy system. The supersaturation data of Lee and Hunt [65] when the first pore appeared are presented in Figure 4. The maximum level of hydrogen supersaturation increases with decreasing solidification time (higher solidification rate), which is consistent with the calculations of Han and Viswanathan [66], regardless of whether the alloy is grain refined or not. The data show consistent scatter between the curve indicated for maximum data and horizontal line for hydrogen solubility.

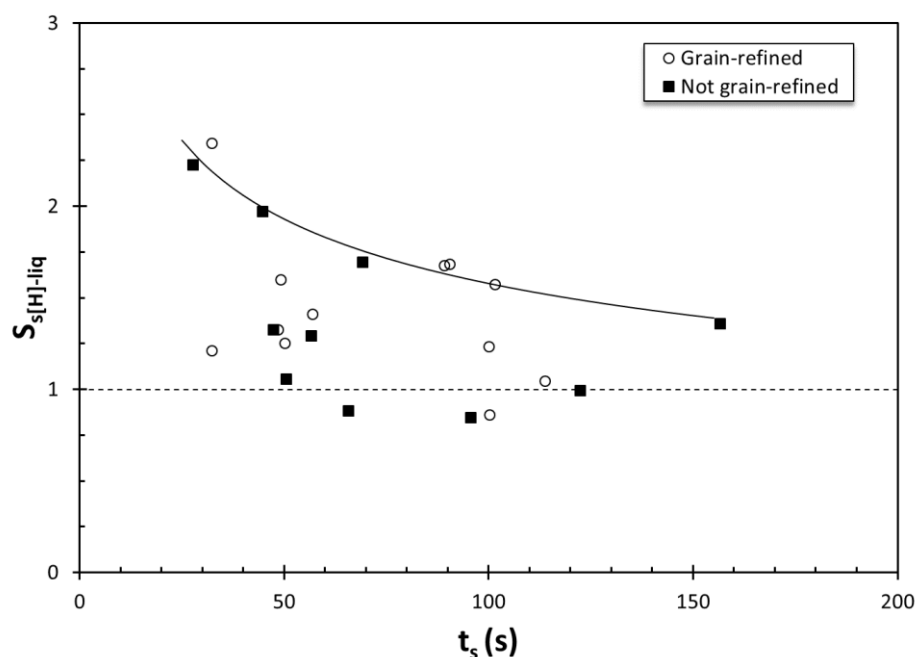


Figure 4. The change in hydrogen supersaturation in an Al-10wt.%Cu alloy at the formation of the first hydrogen pore, with solidification time, with and without grain refining additions (data from Ref. [65]).

The distribution of hydrogen supersaturation at the formation of the first pore can be characterized by using the distribution of the pore formation temperature, as presented in Figure 3 along with Equations (7) and (8). The hydrogen supersaturation distribution is presented in Figure 5. Note that a large majority (94.1%) of the supersaturation values calculated from the pore formation distribution is between 1.0 and 1.5.

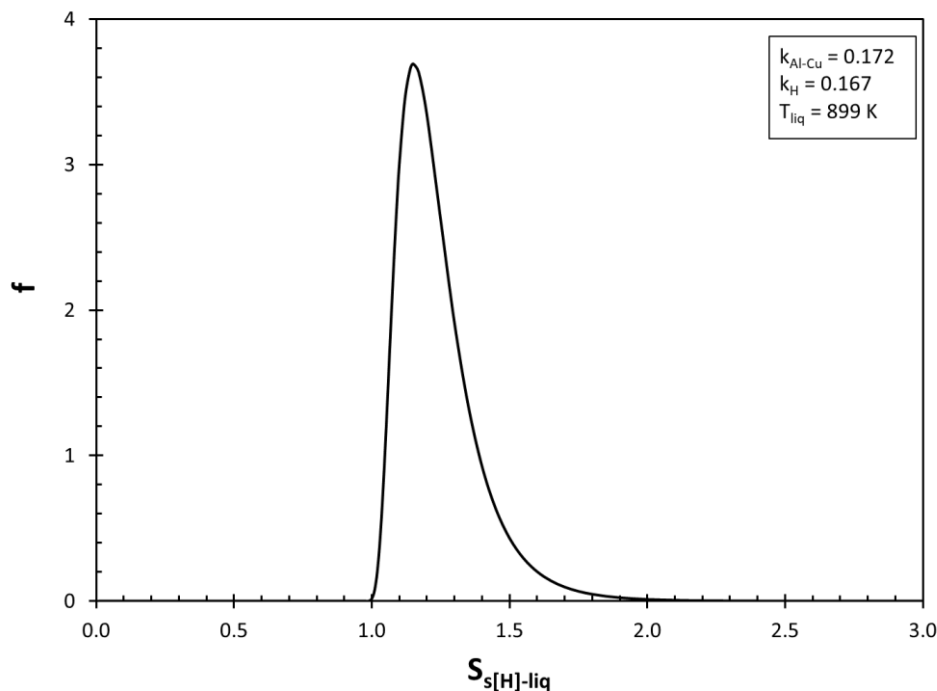


Figure 5. The lognormal distribution for hydrogen supersaturation, as calculated by using Equation (7) and temperature distribution in Figure 3. The parameters used in the calculations are also indicated.

In Figure 3, it is also noteworthy that in three instances, pores were observed to form below the solubility level of hydrogen. These three outliers are, nevertheless, consistent with the results of Lei et al. [67] who investigated pore formation in situ during directional solidification of Al-7wt.%Si and Al-12wt.%Si alloys. They observed that pores appeared in the liquid at a distance of approximately 15 mm from the eutectic solid–liquid interface, where the hydrogen supersaturation is usually expected to be quite low. Similar results have also been reported by Liao et al. [68] who reported that hydrogen pores form well ahead of the directional solidification front in an A356 alloy. Therefore, the assumption of instantaneous pore formation at the point of hydrogen supersaturation in liquid aluminum, without any surface energy barrier, is supported by experimental observations. The root cause of the contradiction between the classical nucleation theory and experimental observations will be addressed later.

4.2. Hydrogen Supersaturation in Solid Aluminum

Thomas and Gruzleski [69] analyzed data from the literature as well as their own data on the effect of hydrogen content of the melt on volume percent of pores in aluminum alloy castings. They reported linear trends for the datasets that they analyzed. The main finding of the study by Thomas and Gruzleski was that the lines did not go through the origin, and extrapolation of the trends yielded positive x-axis intercepts. These intercepts were interpreted as the threshold hydrogen level below which no pore would be expected to form in aluminum castings. Trends to seven datasets from the literature [30,69–73] are plotted in Figure 6, following the same format used by Thomas and Gruzleski. Results show that (i) x-axis intercept, i.e., threshold hydrogen level, varies approximately between 0.1 and 0.2 mL/100 g.Al, and (ii) the slope of trends varies significantly between datasets. The threshold

hydrogen values in Figure 6 are above the hydrogen solubility in solid aluminum or aluminum alloy and imply hydrogen supersaturation in solid aluminum. However, the reasons for the scatter in the slopes and the x-axis intercepts have not been discussed in the literature, to the author's knowledge. This will be addressed now.

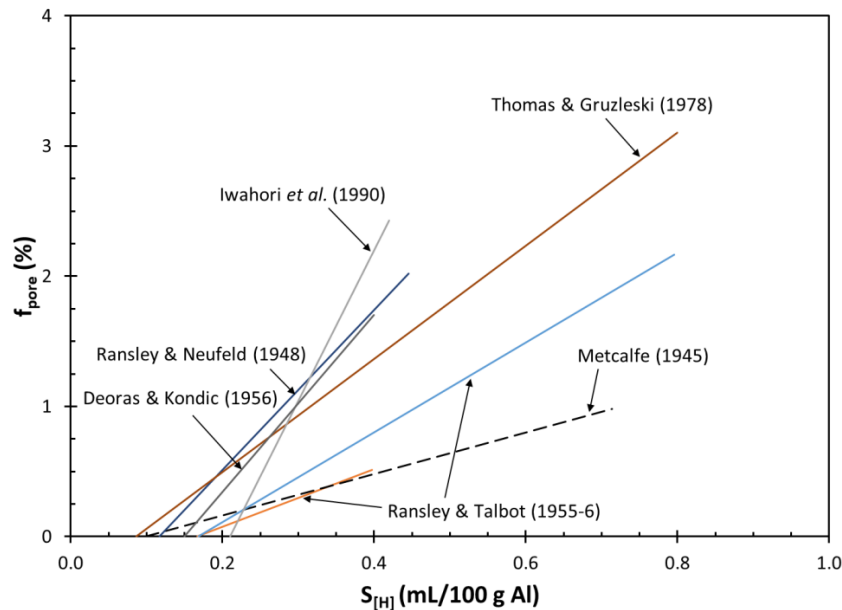


Figure 6. The change in pore volume percent with hydrogen content in the melt from various studies on aluminum castings replotted following the threshold hydrogen concept proposed by Thomas and Gruzleski [69].

Chen and Gruzleski [74] investigated the effect of melt quality and hydrogen content on pore formation in 356 and 319 alloys. To determine melt quality, they forced a portion of the melt to go through a ceramic filter and subsequently quantified the number of inclusions, $N_{A(i)}$, caught in the filter. The data reported by Chen and Gruzleski have been reanalyzed and reinterpreted in this study. The effect of the hydrogen content on pore volume percentage for two melt quality levels is presented in Figure 7. Note that with decreasing melt quality (increasing $N_{A(i)}$), the threshold hydrogen level (x-axis intercept) decreases whereas the slope of the linear relationship, i.e., sensitivity to hydrogen content in the melt, increases. Hence, the amount of spinels and oxides affects the threshold hydrogen content and also the sensitivity of amount of pore formation to hydrogen content.

The relationship between the number of inclusions caught in the ceramic filter and the number density of pores in the 356 alloy castings is presented in Figure 8a. The direct relationship between the number of inclusions and number density of pores in 356 castings is another confirmation of bifilm theory developed by Prof. John Campbell over five decades of research [11,12,50,75–84]. The bifilm theory states that the surface oxide film, when disturbed, folds over itself and gets entrained into the bulk liquid metal. Because dry sides of the oxide are in contact with each other, there is virtually no bonding between the two layers. The result is an entrainment defect which is a crack which opens up during solidification when a negative pressure builds up and/or hydrogen rejected from solidifying metal diffuses into the bifilms and inflates them, like balloons. This mechanism is the only one in which there is no surface energy barrier to be overcome, consistent with the observations in in-situ studies, as discussed above. Hence, the bifilm theory by Campbell is the only explanation for the weakening mechanism in liquid metals. Further evidence is provided in Figure 8b where the combined effect of the number of inclusions (bifilms) and hydrogen content on pore volume percentage is presented. Increasing hydrogen content shifts the curves upward. Moreover, all curves can be extrapolated to the origin, indicating that it is possible to obtain no pores, regardless of the hydrogen level, if there are no bifilms in the metal, it is difficult for hydrogen pores to form, which is consistent with the recent

findings of Dispinar et al. [85] and Griffiths and Raiszadeh [86], as well as the early pioneering work on reduced pressure tests by Brondyke and Hess [87] that the effect of hydrogen on pore formation in an Al-4%Cu alloy is dependent on the oxide content of the melt. We will address the results of this study later.

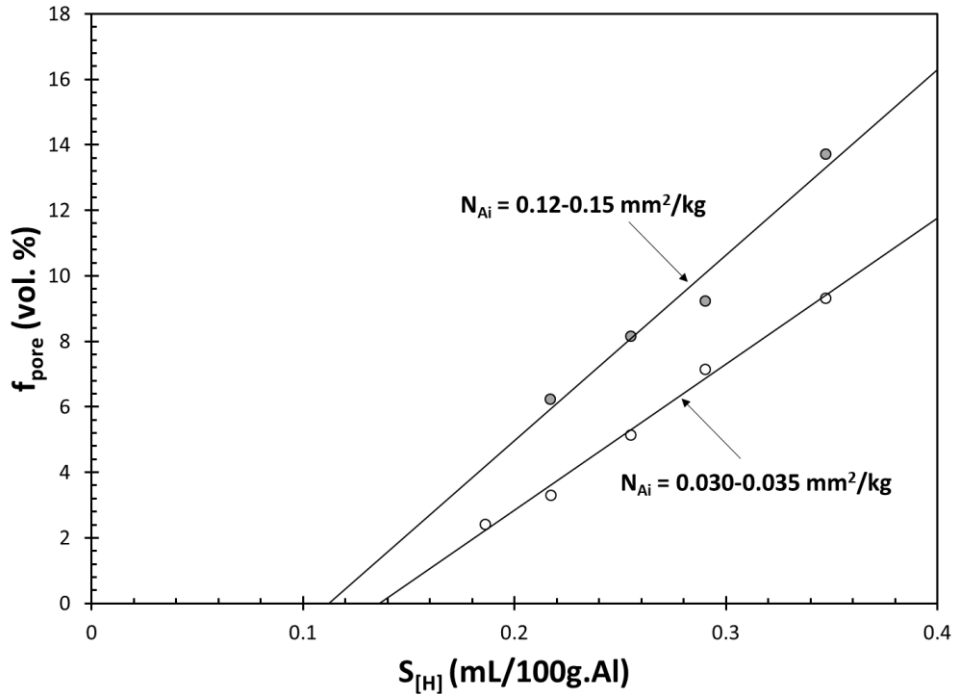
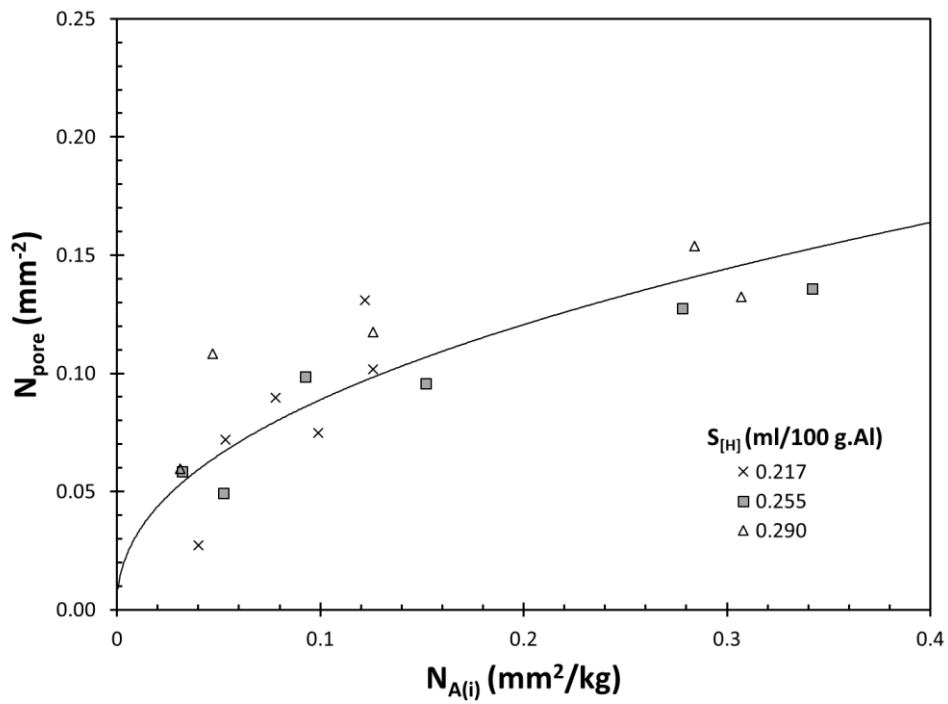


Figure 7. The change in pore volume percent with hydrogen content in the melt for two levels of oxide inclusions (data are from Ref. [74]).



(a)

Figure 8. Cont.

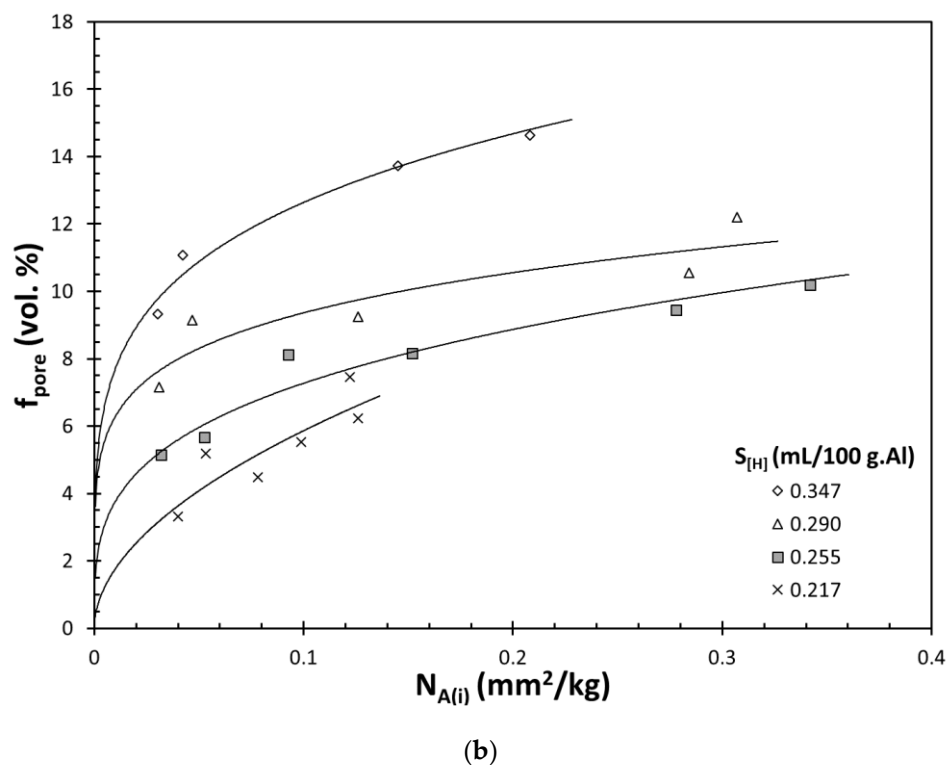


Figure 8. The change in (a) pore number density and (b) pore volume percent with number density of entrainment defects and hydrogen content in the melt in A356 aluminum alloy castings (data are from Ref. [74]).

In a recent study [88], pores in reduced pressure test samples of an A356 alloy were evaluated by scanning electron microscopy. Pores were found to be initiated by entrainment defects, i.e., oxide bifilms, as expected. However, there were many inactive bifilms between dendrites both in the vicinity and away from pores. These bifilms were visible only in x-ray maps and would remain unnoticed in routine analysis. When hydrogen content is increased, a lower number of bifilms can be expected to remain inactive. Therefore, hydrogen can be interpreted and used as an agent that makes preexisting damage to the metal, bifilms, visible, at least partially. We will now reach into several studies in the literature with extreme data on both ends of the spectrum to discuss the combined effect of hydrogen content and entrainment damage (bifilm content) on pore formation.

5. Extreme Data from the Literature and Their Interpretation

5.1. Extreme Damage

Kumar et al. [89] investigated foaming of pure aluminum, Al-5%Mg and Al-9%Si-5%Mg alloys under a reduced pressure of 2×10^{-4} atmosphere. They stirred the melts for twenty minutes, which raised entrainment damage. In two of the melts, they also added 5% SiO_2 particles with an average size of $44 \mu\text{m}$. In all cases, the volume pore percentage was about 80%. The melts were so damaged that neither the chemical composition, and therefore the solidification characteristics, nor the addition of SiO_2 particles had any effect on the pore volume percent. These results clearly demonstrate the overwhelming effect of entrainment damage on pore formation in aluminum alloys.

5.2. Extreme Cleanness

Brondyke and Hess [87] investigated the effect of hydrogen content in the melt, the level of reduced pressure during solidification along with the effect of filtering through a deep bed of alumina particles [90] on the density of an 2014 (Al-4%Cu) alloy. Their density results have been analyzed and

converted to volume pore fraction in the present study, by taking the density above which no pores can be assumed to be present in the alloy as 2700 kg/m^3 , as suggested by Brondyke and Hess. The results of the analysis are presented in Figure 9. Note that deep bed filtering had a dramatic effect on the level of pore formation regardless of the level of reduced pressure. For instance, for a hydrogen content of 0.19 mL/100 g Al , a volume pore percentage of approximately 20% was observed in unfiltered specimens whereas no pores were detected after filtering, as seen in Figure 9a. Similarly, at a reduced pressure of 0.67 kPa (0.0066 atm), a hydrogen content of 0.30 mL/100 g Al could produce approximately 30 vol. % pores in unfiltered specimens and zero pores in filtered specimens, as shown in Figure 9b.

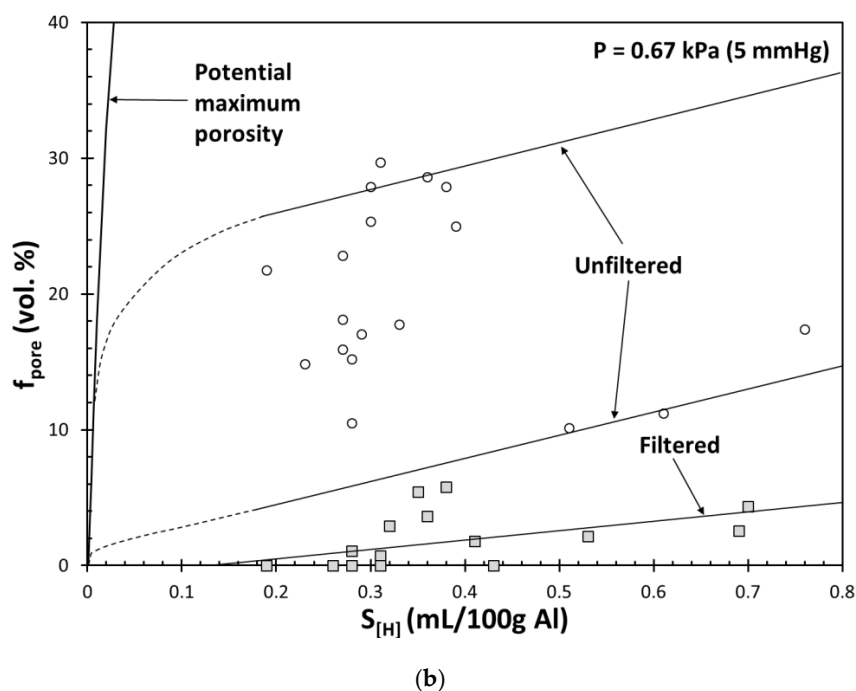
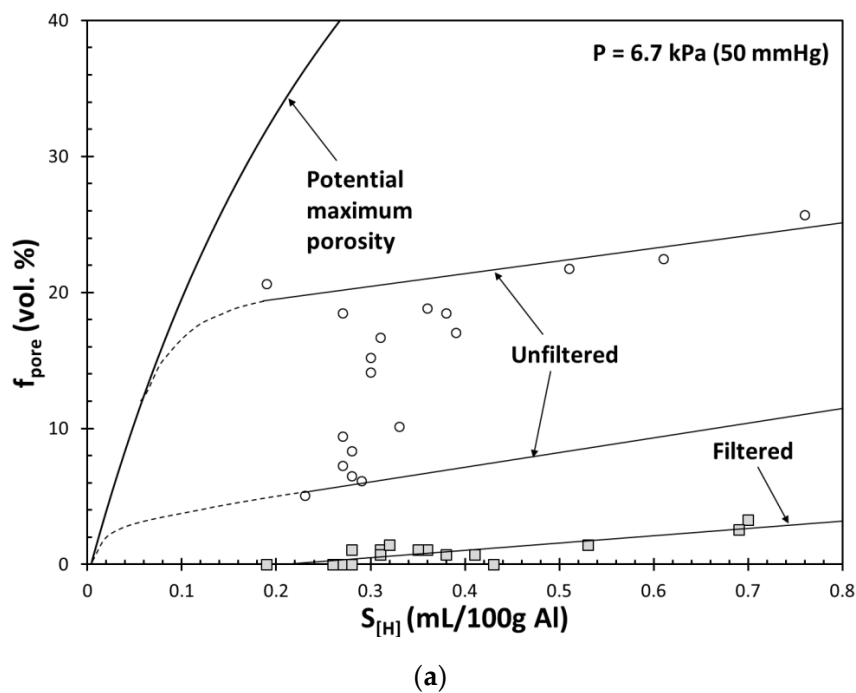


Figure 9. The effect of deep bed filtering and hydrogen content on (a) the density, and (b) the volume percent of pores in an Al-Cu alloy solidified under a reduced pressure of 6.7 kPa (data from Ref. [87]).

In Figure 9a,b, the curves for potential maximum porosity are indicated. These curves have been calculated based on the assumptions that (i) all hydrogen in excess of the solubility in solid aluminum at the solidus temperature forms pores, and (ii) there is no energy barrier to be overcome for pore formation, consistent with several studies in the literature. Following the format of Thomas and Gruzleski, the x-intercept for unfiltered specimens in Figure 9 is not clear and there seem to be an upper and a lower limit to the scatter in unfiltered data, as shown in Figure 9. The scatter in unfiltered and filtered data seems to increase with the decreasing pressure. The lines drawn for upper and lower bounds of the data from unfiltered specimens approach the potential maximum porosity curves. There is, however, a clear x-intercept for filtered specimens for both levels of reduced pressure; 0.22 mL/100 g.Al for 6.7 kPa (0.066 atm) and 0.14 mL/100g.Al for 0.67 kPa (0.0066 atm). More importantly, there are several data points in both conditions that lie on the x-axis, i.e., no pores were detected, at least through the density tests. We will now focus on these points as well as several others from the literature [30,73]. Note that these are actual experimental data, rather than extrapolations to determine x-axis intercepts.

The analysis of extreme data from clean melts is summarized in Table 1. Note that the hydrogen contents of the melt are listed along with the solid solubility at the solidus temperature of the alloy. For Al-Cu alloys, solid solubility was calculated at the eutectic temperature of 548 °C for pure aluminum following the non-equilibrium solidification model, and based on the findings of Ichimura et al. [91] who reported that Cu content has no effect on the solubility of hydrogen in solid aluminum for Cu contents less than 5.7 wt.%. For the Al-12%Si alloy, solid solubility was calculated at the eutectic temperature of 577 °C for pure aluminum and subsequently corrected by the interaction coefficient (= 7.3) reported by Anyalebechi [32] for T = 500 °C. Additionally, the solubility of hydrogen in Al-4%Cu alloy used by Brondyke and Hess [87] has been corrected for the reduced pressure by using the Sievert's Law, Equation (1). The calculated hydrogen supersaturation levels are reported in Table 1.

Table 1. Extreme data from the literature in which no pores were detected along with the associated hydrogen level, calculated hydrogen solubility and hydrogen supersaturation in solid aluminum.

Ref.	Alloy	$S_{[H]}$ (mL/100g.Al)	$S_{[H]eq(sol)}$ (mL/100g.Al)	$S_{s(sol)}$	Notes
[30]	Al-12%Si	0.252	0.153	1.65	$p = 101.3 \text{ kPa (1 atm)}$
	Pure Al	0.513	0.042	12.3	
		0.625		14.9	
[73]	Al-4.6%Cu	0.093	0.016	5.8	$p = 101.3 \text{ kPa}$
		0.19		46.3	
		0.26		63.4	
		0.27		65.8	
		0.28		68.3	
[87]	Al-4.0%Cu	0.43	0.0016	104.8	$p = 0.67 \text{ kPa}$ (0.0066 atm)
		0.19		146.5	
		0.26		200.5	
		0.27		208.2	
		0.28		215.9	
		0.43		331.5	

Note that, for specimens that solidified under atmospheric pressure, a maximum hydrogen supersaturation of 14.9 was found. For specimens under reduced pressure, however, much higher supersaturation levels are reported. It should be noted that these numbers should be taken as “missing”

data, i.e., pores did not form, and hence the liquid metal withstood the supersaturation and any negative pressure formed during solidification. Therefore, the data should be treated as censored, analogous to “run-outs” in fatigue testing. Hence, aluminum can accommodate large amounts of hydrogen remaining in solution above its solubility in the absence of entrainment defects, which is completely in agreement with the findings reported in the literature that it is possible to retain large amounts of hydrogen in vacancies in solid aluminum, as discussed previously.

We can therefore conclude that if the aluminum melt were free from bifilms, it would be unnecessary to measure hydrogen, and no degassing procedure and equipment would be needed. Hydrogen can even be used as a tool to make any damage to the metal visible. It would then be practical to dissolve maximum level of hydrogen in aluminum and yet require no pores to be formed as a condition for defining high quality in a casting quality specification, as suggested by Prof. John Campbell [34]. A fundamental change in how hydrogen is viewed is needed to produce high integrity aluminum castings.

6. Conclusions

- It is impossible for hydrogen to nucleate homogeneously or heterogeneously in liquid aluminum.
- In situ experiments in the literature on pore formation in aluminum showed that pores can form away from the solid-liquid interface and/or when the supersaturation and pressure inside the pores are low, indicating no surface energy barrier to be overcome.
- There is only one mechanism in which the surface energy barrier does not exist so that hydrogen pores can form at the point of supersaturation. This mechanism is the bifilm theory introduced by Prof. John Campbell. Due to the presence of bifilms with two unbonded interfaces, nucleation is bypassed during pore formation. Hydrogen diffuses to oxide bifilms and inflates them. Hence, hydrogen serves as an agent to make entrainment defects visible.
- Without bifilms, high levels of hydrogen supersaturation, as high as 332, in solid aluminum have been reported.
- When entrainment defects are eliminated, it would be unnecessary to measure or control hydrogen levels in the melt. It would even be practical to require a maximum level of hydrogen to be dissolved in aluminum and yet require that no pore be formed in the casting, as a quality control procedure.

Funding: This research received no external funding.

Acknowledgments: The author would like to thank John Campbell for his review and comments on the manuscript.

Conflicts of Interest: The author declares no conflict of interest.

References

1. Tiryakioğlu, M.; Campbell, J.; Staley, J.T. The influence of structural integrity on the tensile deformation of cast Al-7wt.%Si-0.6wt.%Mg alloys. *Scr. Mater.* **2003**, *49*, 873–878. [[CrossRef](#)]
2. Tiryakioğlu, M.; Campbell, J.; Staley, J.T. Evaluating structural integrity of cast Al-7% Si-Mg alloys via work hardening characteristics: I. Concept of target properties. *Mater. Sci. Eng. A* **2004**, *368*, 205–211. [[CrossRef](#)]
3. Tiryakioğlu, M.; Staley, J.T.; Campbell, J. Evaluating structural integrity of cast Al-7% Si-Mg alloys via work hardening characteristics: II. A new quality index. *Mater. Sci. Eng. A* **2004**, *368*, 231–238. [[CrossRef](#)]
4. Tiryakioğlu, M.; Staley, J.T.; Campbell, J. The effect of structural integrity on the tensile deformation characteristics of A206-T71 alloy castings. *Mater. Sci. Eng. A* **2008**, *487*, 383–387. [[CrossRef](#)]
5. Tiryakioğlu, M.; Campbell, J. Ductility, structural quality, and fracture toughness of Al-Cu-Mg-Ag (A201) alloy castings. *J. Mater. Sci. Technol.* **2009**, *25*, 784–789. [[CrossRef](#)]
6. Tiryakioğlu, M.; Campbell, J.; Alexopoulos, N.D. Quality indices for aluminum alloy castings: A critical review. *Metall. Mater. Trans. B* **2009**, *40*, 802–811. [[CrossRef](#)]
7. Tiryakioğlu, M.; Campbell, J.; Alexopoulos, N.D. On the ductility of cast Al-7 pct Si-Mg alloys. *Metall. Mater. Trans. A* **2009**, *40*, 1000–1007. [[CrossRef](#)]

8. Tiryakioğlu, M.; Campbell, J.; Alexopoulos, N.D. On the ductility potential of cast Al–Cu–Mg (206) alloys. *Mater. Sci. Eng. A* **2009**, *506*, 23–26. [[CrossRef](#)]
9. Surappa, M.K.; Blank, E.; Jaquet, J.C. Effect of macro-porosity on the strength and ductility of cast Al-7Si-0.3Mg alloy. *Scr. Metall.* **1986**, *20*, 1281–1286. [[CrossRef](#)]
10. Dai, X.; Yang, X.; Campbell, J.; Wood, J. Effects of runner system design on the mechanical strength of Al-7Si-Mg alloy castings. *Mater. Sci. Eng. A* **2003**, *354*, 315–325. [[CrossRef](#)]
11. Mi, J.; Harding, R.A.; Campbell, J. Effects of the entrained surface film on the reliability of castings. *Metall. Mater. Trans. A* **2004**, *35*, 2893–2902. [[CrossRef](#)]
12. Dai, X.; Yang, X.; Campbell, J.; Wood, J. Influence of oxide film defects generated in filling on mechanical strength of aluminium alloy castings. *Mater. Sci. Technol.* **2004**, *20*, 505–513. [[CrossRef](#)]
13. Green, N.; Campbell, J. Statistical distributions of fracture strengths of cast Al-7Si-Mg alloy. *Mater. Sci. Eng. A* **1993**, *173*, 261–266. [[CrossRef](#)]
14. Tiryakioğlu, M. On estimating the fracture stress and elongation of Al-7%Si-0.3%Mg alloy castings with single pores. *Mater. Sci. Eng. A* **2010**, *527*, 4546–4549. [[CrossRef](#)]
15. Tiryakioğlu, M.; Campbell, J. Quality index for aluminum alloy castings. *AFS Trans.* **2013**, *13*, 217–222. [[CrossRef](#)]
16. Tiryakioğlu, M. Tensile Deformation, Fracture and Hhardness Characteristics of Cast Al-7wt.%Si-Mg Alloys. Ph.D. Thesis, University of Birmingham, Birmingham, UK, 2002.
17. Staley, J.T., Jr.; Tiryakioğlu, M.; Campbell, J. The effect of hot isostatic pressing (hip) on the fatigue life of A206-T71 aluminum castings. *Mater. Sci. Eng. A* **2007**, *465*, 136–145. [[CrossRef](#)]
18. Özdeş, H.; Tiryakioğlu, M. The effect of structural quality on fatigue life in 319 aluminum alloy castings. *J. Mater. Eng. Perform.* **2017**, *26*, 736–743. [[CrossRef](#)]
19. Tiryakioğlu, M.; Campbell, J.; Nyahumwa, C. Fracture surface facets and fatigue life potential of castings. *Metall. Mater. Trans. B* **2011**, *42*, 1098–1103. [[CrossRef](#)]
20. Tiryakioğlu, M. On fatigue life variability in cast Al-10% Si-Mg alloys. *Adv. Mater. Sci. Eng. A* **2010**, *527*, 1560–1564. [[CrossRef](#)]
21. Tiryakioğlu, M. On the relationship between elongation and fatigue life in A206-T71 aluminum castings. *Adv. Mater. Sci. Eng. A* **2014**, *601*, 116–122. [[CrossRef](#)]
22. Tiryakioğlu, M. On the relationship between statistical distributions of defect size and fatigue life in 7050-T7451 thick plate and A356-T6 castings. *Adv. Mater. Sci. Eng. A* **2009**, *520*, 114–120. [[CrossRef](#)]
23. Tiryakioğlu, M. Relationship between defect size and fatigue life distributions in Al-7 pct Si-Mg alloy castings. *Metall. Mater. Trans. A* **2009**, *40*, 1623–1630. [[CrossRef](#)]
24. Nyahumwa, C.; Green, N.R.; Campbell, J. Influence of casting technique and hot isostatic pressing on the fatigue of an Al-7Si-Mg alloy. *Metall. Mater. Trans. A* **2001**, *32*, 349–358. [[CrossRef](#)]
25. Farup, I.; Drezet, J.-M.; Rappaz, M. In situ observation of hot tearing formation in succinonitrile-acetone. *Acta Mater.* **2001**, *49*, 1261–1269. [[CrossRef](#)]
26. Nakajima, H. *Porous Metals with Directional Pores*; Springer: Tokyo, Japan, 2013.
27. Sieverts, A. Absorption of gases by metals. *Z. Metallkunde* **1929**, *21*, 37–46.
28. Liu, H.; Bouchard, M.; Zhang, L. An experimental study of hydrogen solubility in liquid aluminium. *J. Mater. Sci.* **1995**, *30*, 4309–4315. [[CrossRef](#)]
29. Feichtinger, H.; Morach, R. Solubility of hydrogen in molten aluminum at high pressures. *Aluminium* **1987**, *63*, 181–187.
30. Ransley, C.; Neufeld, H. The solubility of hydrogen in liquid and solid aluminium. *J. Inst. Met.* **1948**, *74*, 599–620.
31. Tiryakioğlu, M. Solubility of hydrogen in liquid aluminium: Reanalysis of available data. *Int. J. Cast Met. Res.* **2019**, *32*, 315–318. [[CrossRef](#)]
32. Anyalebechi, P. Analysis and thermodynamic prediction of hydrogen solution in solid and liquid multicomponent aluminum alloys. In *Essential Readings in Light Metals*; Grandfield, J.F., Eskin, D.G., Eds.; Springer: Basel, Switzerland, 2016; Volume 3, pp. 185–200.
33. Tiryakioğlu, M. The myth of hydrogen pores in aluminum castings. In *Shape Casting: 7th International Symposium Celebrating Prof. John Campbell's 80th Birthday*; Tiryakioğlu, M., Griffiths, W., Jolly, M., Eds.; Springer: Basel, Switzerland, 2019; pp. 143–150.

34. Campbell, J. *Complete Casting Handbook: Metal Casting Processes, Metallurgy, Techniques and Design*; Elsevier Science: Amsterdam, The Netherlands, 2015.
35. Yamamoto, T.; Komarov, S.V. Development of a numerical model for hydrogen bubble generation, dynamics and trapping during solidification of aluminium alloys through eulerian-lagrangian framework. *Int. J. Cast Met. Res.* **2019**, *32*, 266–277. [[CrossRef](#)]
36. Poirier, D.R.; Yeum, K.; Maples, A.L. A thermodynamic prediction for microporosity formation in aluminum-rich Al-Cu alloys. *Metall. Trans. A* **1987**, *18*, 1979–1987. [[CrossRef](#)]
37. Carlson, K.D.; Lin, Z.; Beckermann, C. Modeling the effect of finite-rate hydrogen diffusion on porosity formation in aluminum alloys. *Metall. Mater. Trans. B* **2007**, *38*, 541–555. [[CrossRef](#)]
38. Stefanescu, D.M. Computer simulation of shrinkage related defects in metal castings—A review. *Int. J. Cast Met. Res.* **2005**, *18*, 129–143. [[CrossRef](#)]
39. Stefanescu, D.M.; Catalina, A.V. Physics of microporosity formation in casting alloys—Sensitivity analysis for Al–Si alloys. *Int. J. Cast Met. Res.* **2011**, *24*, 144–150. [[CrossRef](#)]
40. Zhu, J.D.; Ohnaka, I. Computer simulation of interdendritic porosity in aluminum alloy ingots and casting. *Model. Cast. Weld. Adv. Solidif. Process.* **1991**, *V*, 435–442.
41. Kubo, K.; Pehlke, R.D. Mathematical modeling of porosity formation in solidification. *Metall. Trans. B* **1985**, *16*, 359–366. [[CrossRef](#)]
42. Katzarov, I.; Popov, J. Pore formation in hot spots. *Int. J. Heat. Mass. Transfer.* **1996**, *39*, 2861–2867. [[CrossRef](#)]
43. Conley, J.G.; Huang, J.; Asada, J.; Akiba, K. Modeling the effects of cooling rate, hydrogen content, grain refiner and modifier on microporosity formation in al a356 alloys. *Mater. Sci. Eng. A* **2000**, *285*, 49–55. [[CrossRef](#)]
44. Huang, J.; Conley, J.G.; Mori, T. Simulation of microporosity formation in modified and unmodified a356 alloy castings. *Metall. Mater. Trans. B* **1998**, *29*, 1249–1260. [[CrossRef](#)]
45. Tiryakioğlu, M. On the intrinsic fracture pressure of liquid and solid aluminum around its melting temperature. *Metall. Mater. Trans. A* **2018**, *49*, 5953–5955. [[CrossRef](#)]
46. Erzi, E.; Tiryakioğlu, M. On the fracture pressure of liquid metals. *J. Mater. Sci. Technol.* **2019**, *35*, 1656–1659. [[CrossRef](#)]
47. Lu, H.; Jiang, Q. Surface tension and its temperature coefficient for liquid metals. *J. Phys. Chem. B* **2005**, *109*, 15463–15468. [[CrossRef](#)] [[PubMed](#)]
48. Biloni, H.; Boettinger, W.J. Solidification. In *Physical Metallurgy I*; Cahn, R.W., Haasen, P., Eds.; Elsevier: Amsterdam, The Netherlands, 1996; Volume 1, pp. 669–842.
49. Tiryakioğlu, M. On the Heterogeneous Nucleation Pressure for Hydrogen Pores in Liquid Aluminium. *Int. J. Cast Met. Res.* submitted.
50. Campbell, J. Entrainment defects. *J. Mater. Sci. Technol.* **2006**, *22*, 127–145. [[CrossRef](#)]
51. Shahani, H.; Fredriksson, H. On the mechanism of precipitation of pores in melts. *Scand. J. Metall.* **1985**, *14*, 316–320.
52. Yousefian, P.; Tiryakioğlu, M. Pore formation during solidification of aluminum: Reconciliation of experimental observations, modeling assumptions, and classical nucleation theory. *Metall. Mater. Trans. A* **2018**, *49*, 563–575. [[CrossRef](#)]
53. Fukai, Y. Superabundant vacancies formed in metal–hydrogen alloys. *Phys. Scr.* **2003**, *2003*, 11. [[CrossRef](#)]
54. Thomas, G.; Willens, R.H. Vacancy concentrations in quenched aluminum. *Acta Metall.* **1966**, *14*, 1385–1390. [[CrossRef](#)]
55. Birnbaum, H.K.; Buckley, C.; Zeides, F.; Sirois, E.; Rozenak, P.; Spooner, S.; Lin, J.S. Hydrogen in aluminum. *J. Alloys Compd.* **1997**, *253–254*, 260–264. [[CrossRef](#)]
56. Ismer, L.; Park, M.S.; Janotti, A.; Van de Walle, C.G. Interactions between hydrogen impurities and vacancies in mg and al: A comparative analysis based on density functional theory. *Phys. Rev. B* **2009**, *80*, 139902. [[CrossRef](#)]
57. Xie, D.; Li, S.; Li, M.; Wang, Z.; Gumbsch, P.; Sun, J.; Ma, E.; Li, J.; Shan, Z. Hydrogenated vacancies lock dislocations in aluminium. *Nat. Commun.* **2016**, *7*, 13341. [[CrossRef](#)]
58. Atwood, R.; Sridhar, S.; Lee, P. Equations for nucleation of hydrogen gas pores during solidification of aluminium seven weight percent silicon alloy. *Scr. Mater.* **1999**, *41*, 1255–1259. [[CrossRef](#)]
59. Atwood, R.C.; Lee, P.D. A three-phase model of hydrogen pore formation during the equiaxed dendritic solidification of aluminum-silicon alloys. *Metall. Mater. Trans. B* **2002**, *33*, 209–221. [[CrossRef](#)]

60. Atwood, R.; Sridhar, S.; Zhang, W.; Lee, P. Diffusion-controlled growth of hydrogen pores in aluminium–silicon castings: In situ observation and modelling. *Acta Mater.* **2000**, *48*, 405–417. [[CrossRef](#)]
61. Lee, P.D.; Sridhar, S. Direct observation of the effect of strontium on porosity formation during the solidification of aluminium–silicon alloys. *Int. J. Cast Met. Res.* **2000**, *13*, 185–198. [[CrossRef](#)]
62. Liao, H.; Song, W.; Wang, Q.; Zhao, L.; Fan, R. Effect of oxide level on pore formation in a356 alloy by X-ray imaging and directional solidification technology. In *ICAA13 Pittsburgh*; Weiland, H., Rollett, A.R., Cassada, W.A., Eds.; Springer: Basel, Switzerland, 2016; pp. 1457–1462.
63. Tiryakioğlu, M. Statistical distributions for the temperature of hydrogen pore nucleation in solidifying aluminium alloys. *J. Mater. Sci. Technol.* **2019**, *35*, 872–874. [[CrossRef](#)]
64. Lee, P.; Hunt, J. Hydrogen porosity in directional solidified aluminium–copper alloys: In situ observation. *Acta Mater.* **1997**, *45*, 4155–4169. [[CrossRef](#)]
65. Lee, P.D.; Hunt, J.D. Measuring the nucleation of hydrogen porosity during the solidification of aluminium–copper alloys. *Scr. Mater.* **1997**, *36*, 399–404. [[CrossRef](#)]
66. Han, Q.; Viswanathan, S. Hydrogen evolution during directional solidification and its effect on porosity formation in aluminum alloys. *Metall. Mater. Trans. A* **2002**, *33*, 2067–2072. [[CrossRef](#)]
67. Lei, Z.; Hengcheng, L.; Ye, P.; Qigui, W.; Guoxiong, S. In-situ observation of porosity formation during directional solidification of al-si casting alloys. *Res. Dev.* **2011**, *8*, 14–18.
68. Liao, H.C.; Song, W.; Wang, Q.G.; Zhao, L.; Fan, R.; Jia, F. Effect of sr addition on porosity formation in directionally solidified a356 alloy. *Int. J. Cast Met. Res.* **2013**, *26*, 201–208. [[CrossRef](#)]
69. Thomas, P.M.; Gruzleski, J.E. Threshold hydrogen for pore formation during the solidification of aluminum alloys. *Metall. Trans. B* **1978**, *9*, 139–141. [[CrossRef](#)]
70. Ransley, C.; Talbot, D. Wasserstoff-porosität in metallen unter besonderer berücksichtigung des aluminiums und seiner legierungen. *Z. Metallkunde* **1955**, *46*, 328–337.
71. Iwahori, H.; Yonekura, K.; Yamamoto, Y.; Nakamura, M. Occurring behavior of porosity and feeding capabilities of sodium-and strontium-modified al-si alloys. *AFS Trans.* **1990**, *98*, 167–173.
72. Deoras, B.R.; Kondic, V. Testing the gas content of molten metals in a foundry. *Foundry Trade J.* **1956**, *100*, 361–364.
73. Metcalfe, G.J. Correspondence on sloman’s paper. *J. Inst. Met.* **1945**, *71*, 618–619.
74. Chen, X.-G.; Gruzleski, J. Influence of melt cleanliness on pore formation in aluminium–silicon alloys. *Int. J. Cast Met. Res.* **1996**, *9*, 17–26. [[CrossRef](#)]
75. Campbell, J. Origin of Porosity in Cast Metals. Ph.D. Thesis, University of Birmingham, Birmingham, UK, 1967.
76. Campbell, J. Pore nucleation in solidifying metals. In *Proceedings of the conference on the Solidification of Metals*; Institute of Metals Publication: Brighton, UK, 1968; pp. 18–26.
77. Fox, S.; Campbell, J. Visualisation of oxide film defects during solidification of aluminium alloys. *Scr. Mater.* **2000**, *43*, 881–886. [[CrossRef](#)]
78. Rashid, A.K.M.B.; Campbell, J. Oxide defects in a vacuum investment-cast ni-based turbine blade. *Metall. Mater. Trans. A* **2004**, *35*, 2063–2071. [[CrossRef](#)]
79. Cao, X.; Campbell, J. Oxide inclusion defects in al-si-mg cast alloys. *Can. Metall. Q.* **2005**, *44*, 435–448. [[CrossRef](#)]
80. Campbell, J. An overview of the effects of bifilms on the structure and properties of cast alloys. *Metall. Mater. Trans. B* **2006**, *37*, 857–863. [[CrossRef](#)]
81. Campbell, J. The origin of griffith cracks. *Metall. Mater. Trans. B* **2011**, *42*, 1091–1097. [[CrossRef](#)]
82. Dispinar, D.; Campbell, J. Porosity, hydrogen and bifilm content in al alloy castings. *Mater. Sci. Eng. A* **2011**, *528*, 3860–3865. [[CrossRef](#)]
83. Campbell, J. Cavitation in liquid and solid metals: Role of bifilms. *Mater. Sci. Technol.* **2014**, *31*, 565–572. [[CrossRef](#)]
84. Campbell, J. The consolidation of metals: The origin of bifilms. *J. Mater. Sci.* **2015**, *51*, 96–106. [[CrossRef](#)]
85. Dispinar, D.; Akhtar, S.; Nordmark, A.; Di Sabatino, M.; Arnberg, L. Degassing, hydrogen and porosity phenomena in A356. *Mater. Sci. Eng. A* **2010**, *527*, 3719–3725. [[CrossRef](#)]
86. Griffiths, W.D.; Raiszadeh, R. Hydrogen, porosity and oxide film defects in liquid al. *J. Mater. Sci.* **2009**, *44*, 3402–3407. [[CrossRef](#)]

87. Brondyke, K.J.; Hess, P.D. Interpretation of vacuum gas test results for aluminum alloys. *Trans. Am. Inst. Min. Metall. Metall. Eng.* **1964**, *230*, 1542–1546.
88. Tiryakioğlu, M.; Yousefian, P.; Eason, P.D. Quantification of entrainment damage in a356 aluminum alloy castings. *Metall. Mater. Trans. A* **2018**, *49*, 5815–5822. [[CrossRef](#)]
89. Vinod Kumar, G.S.; Mukherjee, M.; Garcia-Moreno, F.; Banhart, J. Reduced-pressure foaming of aluminum alloys. *Metall. Mater. Trans. A* **2013**, *44*, 419–426. [[CrossRef](#)]
90. Brondyke, K.J.; Stroup, P.T. Filtering Molten Aluminous Metal. CA599558T, 7 June 1960.
91. Ichimura, M.; Sasajima, Y.; Imabayashi, M. Hydrogen solubility in aluminum-copper alloys. *J. Jpn. Inst. Light Met.* **1989**, *39*, 639–645. [[CrossRef](#)]



© 2020 by the author. Licensee MDPI, Basel, Switzerland. This article is an open access article distributed under the terms and conditions of the Creative Commons Attribution (CC BY) license (<http://creativecommons.org/licenses/by/4.0/>).